Regional Myocardial Strain and Function: From Novel Techniques to Clinical Applications

5

Yuchi Han, Walter R. Witschey, Kevin Duffy, and Victor A. Ferrari

Introduction

CMR allows for a highly accurate description of segmental wall motion and quantitation of contractile function. The excellent contrast between the endocardium and blood pool improves measurement of wall thickness, end-diastolic and end-systolic volumes, and LV ejection fraction using steady-state free precession (SSFP) images. Advancement in 3D echocardiography techniques has improved upon limitations of geometric assumption, but additional limitations regarding imaging windows and endocardial definition persist. Computed tomography (CT) has emerged as a new tool to evaluate cardiac function, but the radiation risk and low temporal resolution hamper its value in assessing regional function. CMR has been the noninvasive method of choice for the evaluation of regional myocardial movement since myocardial tagging was invented almost 30 years ago. A number of developments and improvements on the technique have taken place to improve image resolution, quality, three-dimensional image acquisition, and scan time. The purpose of this chapter is to describe the methods and clinical applications of these techniques for assessment of segmental ventricular function.

Y. Han (✉) · K. Duffy · V. A. Ferrari
Cardiovascular Medicine Division, Department of Medicine, Perelman School of Medicine, University of Pennsylvania, Philadelphia, PA, USA
e-mail: yuchi.han@uphs.upenn.edu

W. R. Witschey
Department of Radiology, Perelman School of Medicine, University of Pennsylvania, Philadelphia, PA, USA

Methods and Techniques

Motion Quantification

Analysis of cardiac motion is closely related to engineering principles of continuum mechanics. Many aspects of motion (kinematics) are well beyond the scope of this chapter, and there are many excellent books [1] and reviews [2] on this topic. The discussion here is limited to brief definitions of quantitative motion parameters, such as displacement, strain, and torsion.

From the viewpoint of kinematics, the heart is a continuous material, and its behavior is the summative property of many cardiac myocytes, their extracellular space, and nearby vascular space. This assumption is valid because the MRI spatial scale (voxel volume ~ 1–40 mm^3) is much larger than the microscopic scale. The initial position of cardiac muscle at end-diastole is the reference configuration, and different positions during the cardiac cycle are the deformed configurations. The displacement is the distance and direction of tissue motion between the reference and deformed configuration, and the displacement field is a description of all tissue displacements.

The displacement field is also a spatial map that provides useful information about regional myocardial health. Ischemic tissue may have reduced displacement in regions of impaired contractile function. One shortcoming of the displacement field technique is that it reports both regional and global translation and rotation. Global and regional displacement in opposite directions would be incorrectly interpreted as impaired function without first accounting for global displacement.

Myocardial strain is a parameter derived from displacement that simplifies the analysis of myocardial motion. The concept is that myocardium will undergo local stretching, shortening, or shearing as it transitions from reference

R. Y. Kwong et al. (eds.), *Cardiovascular Magnetic Resonance Imaging*, Contemporary Cardiology,
https://doi.org/10.1007/978-1-4939-8841-9_5

to deformed configurations. Strain quantifies local motion without the influence of confounding global motion. Unlike tissue displacement, which is an absolute quantity, strain may be defined in several ways. For instance, Cauchy strain is a dimensionless quantity defined as the ratio of displacement to a reference length and is expressed as a percentage.

The myocardial displacement is a 3D vector quantity with components u_R, u_C, and u_L, where the subscripts R, C, and L refer to local radial, circumferential, and longitudinal wall coordinates. The Green-Lagrange strain is a tensor quantity (a 3 × 3 matrix)

$$E = \begin{bmatrix} e_{RR} & e_{RC} & e_{RL} \\ e_{CR} & e_{CC} & e_{CL} \\ e_{LR} & e_{LC} & e_{LL} \end{bmatrix},$$

where the diagonal elements quantify stretch or shrink and off-diagonal elements measure shear. Strain could also be reported with respect to the local fiber orientation, also called the principal strain, a diagonal tensor

$$E = \begin{bmatrix} e_{11} & & \\ & e_{22} & \\ & & e_{33} \end{bmatrix}.$$

The velocity and strain rate are the time rate of change of displacement and strain, respectively.

CMR Motion Imaging: Strain and Displacement

Normal myocardial architecture consists of ventricular myocytes organized in helical layers of fiber bundles with a preferential transmural orientation [3–5]. The maximum principal strain e_{11} is presumed to correspond to the myocardial fiber orientation. As will be discussed further, both displacement and strain are readily obtained from tagged MRI and displacement encoding of stimulated echoes (DENSE) MRI techniques.

Magnetic resonance imaging offers multiple advantages to radio-opaque marker [6, 7] or ultrasonic transducer (sonomicrometry) [8, 9] motion tracking for cardiovascular applications, including its noninvasive nature, a closely packed displacement field, and 3D spatial coverage. Numerous MRI methods have been introduced to quantitatively assess regional myocardial function, and the scope of topics is broad, so we refer interested readers to more detailed reviews of MRI methodology [2, 10, 11] and image analysis [10]. This section will focus mainly on tagging, displacement encoding (DENSE), strain encoded (SENC), velocity mapping, and feature tracking MRI techniques.

Myocardial Tagging

Myocardial tagging refers to MR imaging techniques that generate noninvasive deformable lines or grids to track myocardial motion. The imaging sequence employs magnetization preparation for grid encoding followed by cine MRI to monitor grid deformation [12, 13]. Spatial modulation of magnetization (SPAMM) [13] uses a radiofrequency pulse pair and magnetic field gradient to generate deformable lines in one dimension, although multidimensional tags allow for 2D or 3D motion field imaging [14].

Computer vision algorithms extract grid deformation and produce closely packed displacement fields using optical flow [14–16], image registration [17], deformable models, splines [18, 19], and Gabor filters [20]. The displacement field spatial resolution is determined by tag grid density and is larger than the pixel resolution, although most algorithms produce dense displacement fields at native image resolution [14]. To improve upon magnitude image-based motion detection, frequency domain detection, called harmonic phase (HARP) imaging, extracts motion from cardiac phase [21–24].

Validation studies have been performed with sonomicrometry [25, 26] and in vitro systems [27, 28]. Sonomicrometry exhibited reduced circumferential shortening compared to tagging, suggesting that the transducers impaired local function [26].

There are several limitations to myocardial tagging techniques. Tag persistence is associated with myocardial water spin relaxation (T_1 and T_2) and cine pulse sequence parameters. Muscle T_1 is approximately 1 s at 1.5 T, and tags are known to fade in the middle and late diastolic cardiac phases, although it is possible to prolong tag persistence with increased T_1 at a higher magnetic field strength or with complementary [29] (Fig. 5.1) or cascaded [30] SPAMM.

DENSE Imaging

DENSE performs displacement encoding by using a pair of magnetic field gradients separated by a mixing period to spatially encode displacement as MR signal phase information [31]. DENSE displays motion information by regional vectors with motion direction and length representing the magnitude of motion. DENSE provides excellent myocardial border definition since it is based on a black blood sequence and is highly reproducible and quantitatively equivalent to myocardial tagging sequences in in vivo experiments (Fig. 5.2) [32].

SENC Imaging

SENC is a newer variation of the tagging technique. In some ways, it is similar to DENSE as its basis is a stimu-

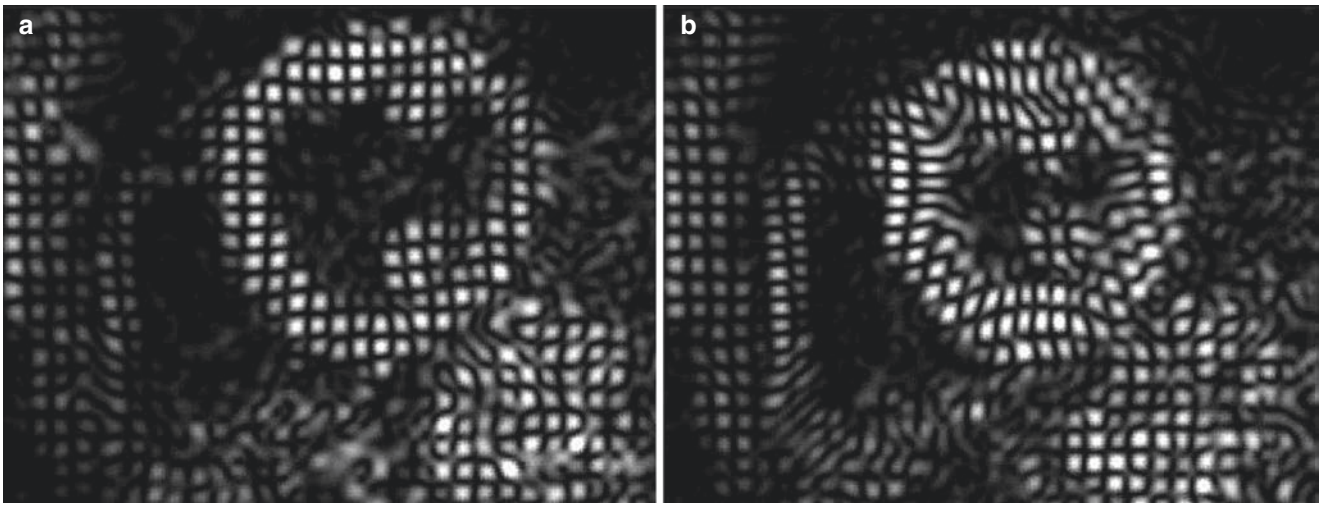

Fig. 5.1 CSPAMM tagging of a subject at end-diastole (**a**) and at end-systole (**b**). Well-adapted CSPAMM sequences provide excellent persistence of tagging into diastole with high spatial and temporal resolution

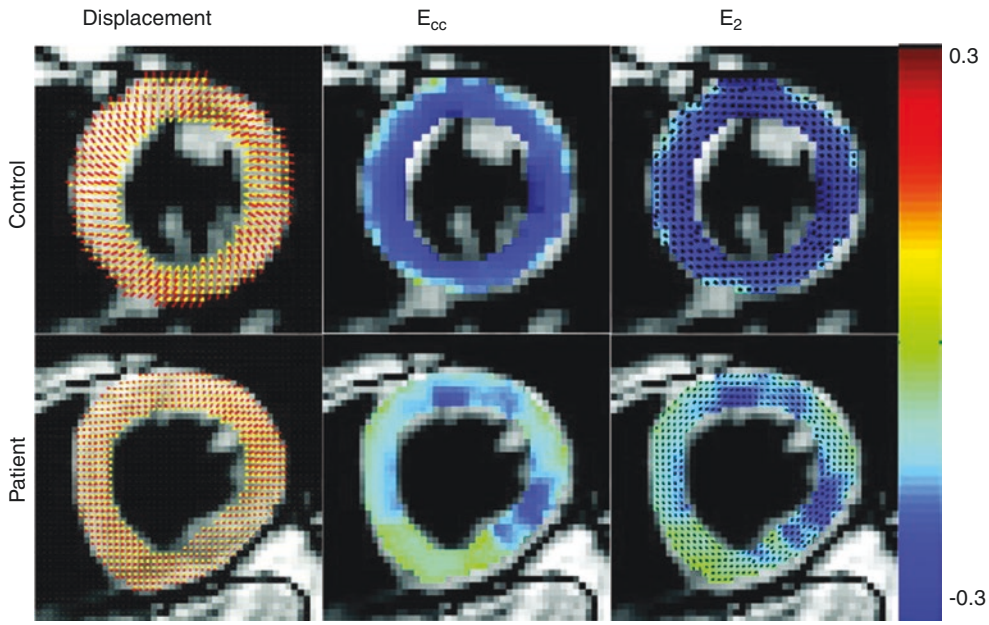

Fig. 5.2 Representative end-systolic (left column) displacement, (middle column) E_{cc}, and (right column) E_2 field maps of a control, as well as those of a 49-year-old male patient with nonischemic cardiomyopathy and ejection fraction of 45%. These examples demonstrate the sensitivity of fast cine DENSE MRI to detect regional variation in contractile function. Compared to the control subject, the patient exhibited considerably lower displacement and magnitude of E_{cc} and E_2 (Reprinted from Feng et al. [32], with permission from John Wiley and Sons)

lated echo acquisition mode pulse sequence, but in contrast to DENSE, the strain information is contained in the magnitude rather than phase images and has the advantages of measuring high-resolution strain with simple post-processing. In contrast to conventional tagging, SENC is applied in the through-plane direction by creating a stack of magnetization-saturated planes that lie inside and parallel to the image plane and therefore obtains a through-plane strain map. SENC has been validated against conventional tagging and has been shown to be accurate and reproducible (Fig. 5.3) [33].

Velocity Encoding

Velocity mapping uses a bipolar magnetic field gradient to encode velocity as MR signal phase information [34, 35]. The maximum encoded velocity, v_{enc}, is set to account for peak anticipated tissue velocity to prevent aliasing. Long acquisition times have hampered clinical application and require prospective respiratory gating to mitigate breathing motion artifacts. New image acquisition and reconstruction strategies may reduce total scan times. Self-gating has been used to derive motion information directly from under-sam-

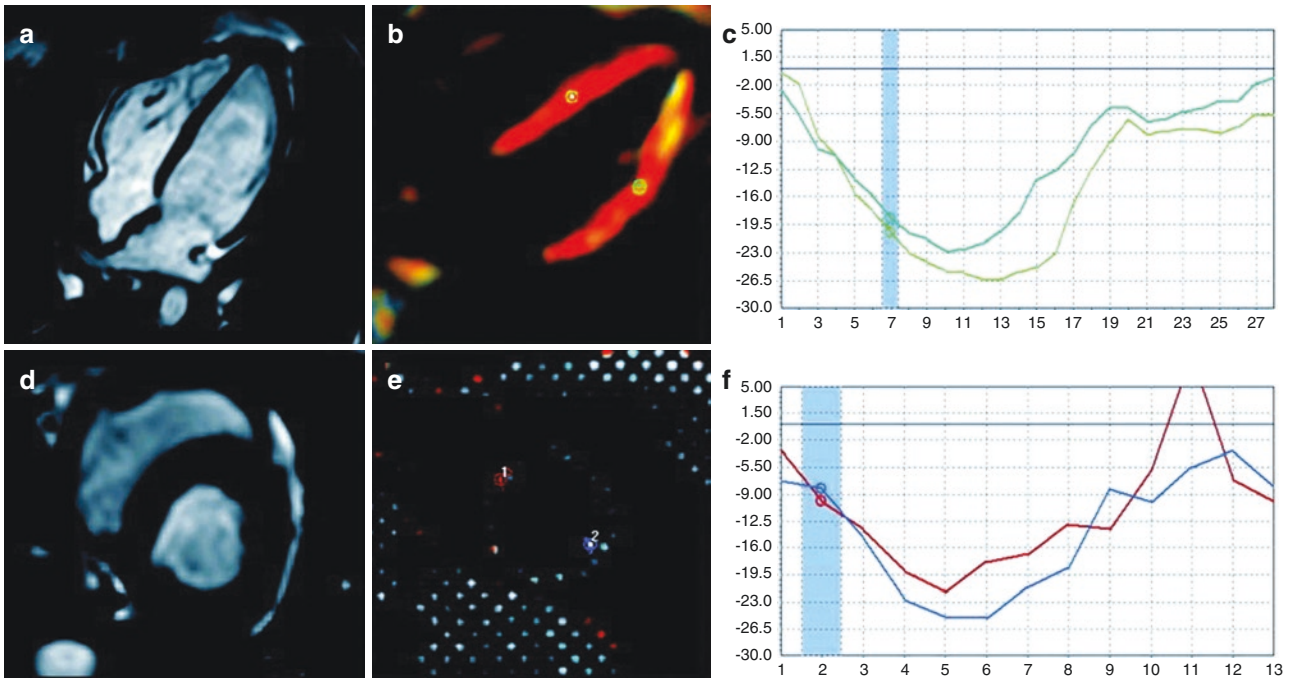

Fig. 5.3 Strain measurements obtained by SENC and MR tagging. (**a**) CINE image (four-chamber view) of a healthy volunteer. (**b**) Color-coded functional SENC image in the same plane orientation. Maximum contraction is illustrated in red. (**c**) The circumferential strain results obtained by SENC. (**d**) CINE image (short-axis view) of the same healthy volunteer. (**e**) Color-coded MR tagging image in the same plane orientation as the short-axis slice (midventricular) for comparison of circumferential strain obtained by MR tagging to SENC imaging as SENC is a technique that uses tag surfaces that are parallel—not orthogonal—to the image plane. (**f**) The circumferential strain results calculated by MR tagging (Reprinted from Neizel et al. [33], with permission from John Wiley and Sons)

pled MR images [36] and may improve scan efficiency and image quality.

Feature Tracking

MR feature tracking (FT) (Fig. 5.4) [37] infers quantitative motion parameters directly from myocardial tissue features, such as contours, trabeculations, and other distinctive cardiac anatomy, with computer vision [38, 39]. Rapid clinical adoption is now possible since several commercial software packages are now available, motion is quantified from cine SSFP images, and no additional MR pulse sequences are required.

Validation studies showed close correlation between FT and tagging using HARP analysis in normal subjects, in Duchenne muscular dystrophy population [40], and in pediatric cancer survivors [41]. Circumferential (e_{CC}) and radial (e_{RR}) LV strain appear to be most reproducible [42]. Radial strain was reported to have the best sensitivity and specificity for detection of postinfarction scar [43]. Reproducibility and strain values from FT algorithms are also reduced when derived from post contrast injection cine images [44].

Feature tracking algorithms are currently not standardized, so discrepancies between software have been reported [45]. Incorporation of myocardial incompressibility constraints may potentially improve robustness and preserve physiologic conditions [46]. Large-scale adoption of this technique and establishing cutoffs to guide clinical practice are hampered by lack of standardization in sequence parameters and analytic tools, but the potential utility of FT continues to expand.

Clinical Applications

Normal Regional Function

The accurate assessment of regional LV function has been improved greatly with myocardial tissue tagging. Lima et al. [25] showed in an animal model that CMR with tissue tagging allows accurate assessment of systolic wall thickening, with good correlation to invasive methods using sonomicrometers. The strongest correlation between MR imaging and percent systolic wall thickening by sonomicrometer crystals is achieved by using the three-dimensional volume element approach, by accounting for obliquity between the image plane and the left ventricular wall.

In the normal human LV, there is transmural heterogeneity of circumferential shortening with endocardial segments > mid wall > epicardial segments and longitudinal heterogeneity of circumferential shortening with apical segments > basal segments [47]. There are also patterns of regional heterogeneity of myocardial contraction and relaxation that

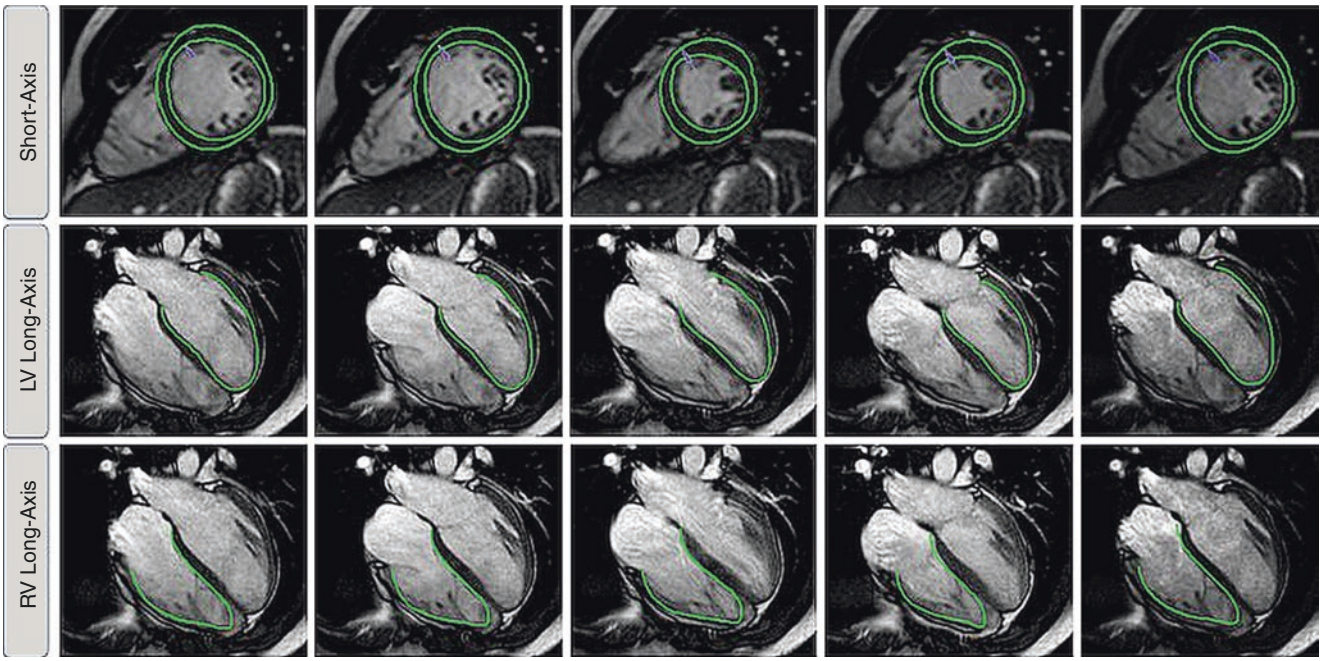

Fig. 5.4 Feature tracking in short-axis and long-axis orientation**.** The figure shows a representative example of the tracking in short-axis and long-axis orientation of the left ventricle (LV) and the right ventricle (RV) (Reprinted from Schuster et al. [37])

occur with aging resulting in increased apical systolic rotation and reduced apical relaxation [48, 49].

CMR has been the gold standard to evaluate the right ventricular (RV) volume and function. The RV myocardial contraction pattern is more difficult to describe as compared to the LV due to its complex shape and its very thin wall, which makes strain analysis more challenging. For the left ventricle, a 2D tag grid can be used to track intersection points within the myocardial wall; however, the RV is too thin for this to be practical. Instead, investigators have used either 1D tags or bidirectional tags with tracking of the intersection of the tag lines with the mid wall of the RV, rather than tracking intersection points of grid lines. New techniques such as SENC are able to provide higher-resolution strain analysis of the RV [50].

For normal RV regional function, increasing regional short-axis shortening from the RV outflow tract to the RV apex has been described using 1D, 2D tagging and SENC [50–52]. Longitudinal contraction is found to be greater at the apex and base, with a decrease in mid-ventricular segments by SENC [50]. The apex also appears to reach peak shortening earlier than mid-ventricular and basal segments [50].

Myocardial Ischemia

Using myocardial tagging in a radial orientation, Azhari and Denisova demonstrated that subendocardial dysfunction was the best discriminant of ischemia [53, 54]. The analysis of wall motion abnormalities with dobutamine stress echocardiography is an established method for detection of myocardial ischemia. CMR has been combined with stress modalities for the evaluation of CAD. Dobutamine CMR with tagging has been shown to detect significantly more new wall motion abnormalities than cine imaging alone in a study of 207 patients with known or suspected CAD [55]. Similarly, combining SENC with dobutamine CMR, Korosoglou et al. demonstrated the incremental value of strain by detecting a significantly larger number of patients with ischemia as compared to wall motion analysis alone [56]. SENC also has been shown to improve the diagnostic accuracy in detecting myocardial ischemia during dobutamine stress at an intermediate dose as compared to cine imaging, using quantitative coronary angiography as the standard of reference [57]. In a study using adenosine triphosphate (ATP) to induce perfusion abnormalities in ischemic segments, circumferential strain by tagging was shown to decrease in ischemic segments, as opposed to nonischemic segments, where circumferential strain increased compared to resting images [58].

Myocardial Infarction

CMR is also an especially good tool for the detection and quantification of myocardial infarction (MI). Infarction is a heterogeneous process involving predominantly the endocardium in smaller infarcts or can be more transmural in more substantial infarcts. An MI can result in multiple

patchy areas of necrosis surrounded by viable myocardium. CMR with tissue tagging can highlight areas of infarction and can also assess the effects of infarction on the non-infarcted regions of the ventricle. Circumferential and longitudinal strains are decreased not only in the infarcted areas but also in the remote zones in patients with reperfused anteroapical infarction [59]. This study also showed increases in the radius of curvature of the ventricular walls in both the infarcted and remote zones. A similar study [60] using tagged CMR and two-dimensional finite element analysis early after anteroapical infarction clearly demonstrated decreased wall strain and reorientation of the short-axis vector of myocardial contraction away from the centroid of the left ventricle. Early after infarction remote zone hyperfunction was seen, indicating a possible compensatory increase in function remote from the infarcted area. Average short- and long-axis strain values decreased to approximately 25% of normal in infarcted regions. A third study [61] demonstrated similar findings of decreased deformation not only in anteroapical MI but also in infarcts of all coronary distributions. Together, these findings imply an increase in segmental wall stress in regions distant from large infarcts resulting in globally decreased function and frequently leading to a post-MI chronic cardiomyopathy.

Microvascular obstruction (MO) is an important predictor of unfavorable remodeling after MI by preventing adequate healing early after myocardial infarction. This phenomenon is also referred to as a "no-reflow" territory as seen after angioplasty of acute infarcts fail to return adequate flow to a vessel. A canine infarct model has been used to explore the relationship of the extent of MO and its effect on regional and global function [62]. Animals with a greater extent of MO had a significantly greater risk of developing unfavorable remodeling within 10 days of infarction as assessed by CMR functional imaging. Myocardial strain decreased significantly in the infarcted regions, and the greater the area of MO within the infarct, the greater the decrease in myocardial strain. Not only was strain decreased in infarcted areas but also in regions adjacent to the infarct with normal perfusion.

Peak systolic circumferential strain measured by SENC is able to differentiate non-transmural from transmural infarcted myocardium with high sensitivity and specificity correlating well with tagging in acute MI [63].

Viability

Assessment of viability is important in the management of ischemic heart disease because revascularization of dysfunctional but viable myocardium can improve function and survival. Traditionally, viability can be assessed through the evaluation of mechanical function (dobutamine echocardiography) or perfusion and metabolism (SPECT and PET). CMR has been developed to also evaluate mechanical function (dobutamine CMR +/− tagging) or perfusion and metabolism (contrast CMR and spectroscopic analysis) in addition to delayed enhancement to assess myocardial viability.

Low-dose dobutamine echocardiography is an established method for the detection of viability. As with dobutamine echocardiography, dobutamine CMR can similarly detect increased function in dysfunctional but viable myocardium. When compared to PET, dobutamine CMR correlates well, with a sensitivity of 88% and a specificity of 87% [64]. Sayad et al. described quantitation of left ventricular wall thickening using CMR with myocardial tagging in patients with segmental wall abnormalities at rest [65]. Each subject underwent CMR scanning with low-dose dobutamine infusion (up to 10 μg/kg/min) at baseline and 4–8 weeks after revascularization. Using CMR with tagging, resting end-diastolic and end-systolic wall thicknesses in abnormal segments at rest were compared with those measured at peak dobutamine and again after revascularization. It was found that end-systolic wall thickness after low-dose dobutamine infusion predicted improvement in segmental function after revascularization. Alternatively, segments with a resting end-systolic wall thickness of <7 mm did not improve after revascularization [65]. 3D myocardial strain analysis using tagging with low-dose dobutamine can also be used to differentiate viable from nonviable myocardium. While at rest, circumferential strain was decreased compared to controls in both the viable and nonviable segments. When compared with resting images, dobutamine stress imaging resulted in an increase in circumferential strain in the viable segments and no change in the nonviable segments [66].

Dobutamine CMR with myocardial tagging can also be used in the setting of revascularized acute myocardial infarction to predict recovery of function. Geskin et al. performed tagged dobutamine CMR studies in 20 patients within an average of 4 days after infarction with revascularization [67]. At approximately 8 weeks, a CMR without dobutamine was performed to assess for recovery of function. Those patients with a normal intramyocardial circumferential segment shortening on the initial study had greater recovery of function on the follow-up CMR.

Hypertrophic Cardiomyopathy

Hypertrophic cardiomyopathy (HCM), an autosomal dominant genetic disease caused by a defect in one of a number of genes of the sarcomere, is characterized by left ventricular hypertrophy and myofibrillar disarray. There are many morphological variants, and frequently the pattern of hypertrophy is asymmetrical. Histologically, patients often have patchy areas of fibrosis, which may be visualized as areas of delayed enhancement [68].

To further characterize contractile function in HCM, Young et al. [69] performed a strain analysis on 2D SPAMM tagging CMR images from 7 HCM and 12 normal volunteers. A 3D finite element model was used to associate the short-axis and long-axis data. On a regional level, strain analysis revealed that circumferential shortening was reduced in the entire septum and most other regions in the HCM patients when compared to the normal controls. While contractile function was reduced, left ventricular torsion in the HCM group was increased by approximately 5° [69].

Similarly, Kramer et al. [70] found prominent regional heterogeneity using 2D tagging in cardiac function in 10 HCM patients with a predominant pattern of asymmetric septal hypertrophy vs. normal subjects. While circumferential shortening was less in the septal, inferior, and anterior walls, it was not significantly different in the lateral wall. At all short-axis levels, circumferential shortening was decreased in HCM, and longitudinal shortening was markedly reduced at the basal septum [70]. A number of reports also describe the association of decreased myocardial strain with areas of delayed enhancement using tagging [71] or feature tracking [72].

Not surprisingly, diastolic function is also abnormal in HCM. Ennis et al. [73] studied eight patients with HCM and found that, in addition to decreased systolic strain, regional diastolic strain was reduced as well. The patients had decreased early diastolic strain rates, indicative of a prolonged early filling phase. The strain rate was then seen to increase during mid-diastole, signifying a continued slow filling phase and abnormal relaxation throughout diastole.

On many levels, HCM appears to be a heterogeneous process, with regional variability in the degree of wall thickness, the pattern of delayed enhancement, and contractile function.

Pressure Overload Left Ventricular Hypertrophy

Patients often develop concentric left ventricular hypertrophy (LVH) as a result of disorders associated with elevated afterload, such as systemic hypertension or aortic stenosis. Compensatory hypertrophy may also lead to contractile dysfunction. Palmon et al. [74] studied 30 patients with hypertension and concentric LVH using SPAMM tagging to more accurately quantitate regional contractile function. Circumferential and longitudinal shortening was depressed by approximately 5–10% when compared to normal volunteers. Unlike the normal volunteers, patients with hypertensive LVH had regional variability with the greatest circumferential shortening occurring in the lateral wall and the least shortening occurring inferiorly.

Patients with concentric LVH and preserved systolic function in large cohort studies such as MESA (Multi-Ethnic Study of Atherosclerosis) were evaluated with CMR. Rosen et al. [75] analyzed tagged CMR studies in 441 such patients with the HARP analysis method and found that, as with previous smaller trials, left ventricular systolic strain was decreased. This reduction in strain had regional variability with a more pronounced effect in the LAD distribution. In another analysis of the MESA patients, Edvardsen et al. [76] studied 218 patients with concentric LVH and found no difference in systolic strain between the LVH patients and the normal controls but found a noticeable difference in diastolic function where the LVH patients had significantly reduced regional diastolic strain rates signifying a more prolonged and slower diastolic relaxation.

Dilated Cardiomyopathy

In the endocardium, both fiber and cross-fiber shortening are greatly reduced in dilated cardiomyopathy (DCM) [77]. Myocardial strain analysis has allowed assessment of mechanical dyssynchrony in DCM which is a key predictor for responsiveness to LV pacing [78]. Regional heterogeneity has been demonstrated in DCM using tagging with the anteroseptum and inferoseptum as most affected segments and the inferolateral wall as the least affected segments as compared to normal [79, 80]. A great majority but not all patients with LBBB demonstrate systolic lengthening in the septum shown by myocardial tagging and consequently greater dyssynchrony compared to non-LBBB patients [81]. There is a decrease in systolic torsion magnitude in DCM in addition to discontinuing counter-clock rotation of the apex before end-systole [82].

Valvular Heart Disease

While the heart valves may be evaluated by CMR through direct visualization of the leaflets and quantification of regurgitation volume through phase contrast methods, the impact of ventricular remodeling with abnormal loading conditions can be best evaluated by CMR.

In the pressure overloaded state of severe aortic stenosis, there are contractile abnormalities as with hypertensive heart disease. Stuber et al. [83] reported in patients with aortic stenosis that torsion was significantly increased and diastole was delayed, as indicated by late peak diastolic untwisting. Similar results were reported by Nagel et al. [84] showing that maximal systolic torsion was increased in the aortic stenosis patients (from 8° to 14°) and that diastolic untwisting was delayed and prolonged. The abnormal pathologic changes associated with the high afterload state of aortic stenosis can actually be reversed, as demonstrated by Sandstede et al. [85] in their study of 12 patients with aortic

stenosis who underwent aortic valve replacement. Compared with eight healthy volunteers, the aortic stenosis patients prior to valve replacement had significantly higher torsion (25° compared to 14°). One year after surgery, the apical torsion had normalized to 16°.

Aortic regurgitation (AR), due to the increased volume and pressure load on the left ventricle, leads to left ventricular dilatation and eccentric hypertrophy. Optimal timing for surgery can be difficult to determine, as patients may remain relatively asymptomatic even as their left ventricle becomes markedly abnormal. The quantification of regional left ventricular function using tagged CMR could potentially detect subtle changes in myocardial function, which could herald the need to replace the aortic valve prior to the development of irreversible LV dysfunction. However, the results of myocardial strain in chronic AR patients are less than useful. Ungacta et al. [86] studied six patients with chronic severe aortic insufficiency using tagging pre and post AVR and showed no difference in various contractile parameters such as global circumferential shortening or radial thickening compared to controls. The postsurgery study 5 months later also showed no significant difference in overall circumferential shortening or radial thickening despite a decrease in LV volume and a return to a more normal ventricular geometry as compared to controls. On a regional basis, however, posterior wall strain was reduced [86]. In a later study of 14 chronic AR patients, [87] the pre-surgery strain was not different compared to controls. At 28 ± 11 months of follow-up post AVR, 3D minimum principal, longitudinal, and circumferential strain were decreased as compared to controls.

Severe mitral regurgitation (MR) can result in abnormal myocardial contractile function, despite having normal global parameters such as ejection fraction. Mankad et al. [88] studied regional strain in seven patients with severe mitral regurgitation before surgery and again approximately 8 weeks after surgery. Prior to surgery, maximum strain (similar to radial thickening) was increased compared to normal and became even greater after surgery. Prior to surgery, minimum strain (comparable to circumferential shortening) was decreased compared to normal and further declined after surgery. Heterogeneity of myocardial longitudinal and circumferential strains are also demonstrated in chronic MR, shown as decreased strain in the LV septum and increased strain in the LV lateral wall in 15 patients with asymptomatic chronic severe MR [89].

Pericardial Disease

The pericardium can be well visualized with CMR, despite having an average thickness of 1.5–2 mm [90]. Differentiating between constrictive pericarditis and restrictive cardiomyopathy can often be difficult; CMR adds additional information in these cases. In addition to more clearly defining the anatomic structure of the pericardium through standard cine CMR imaging, tagged CMR allows the interpreter to discern whether the pericardium is adhered to the heart [91]. In normal hearts, the pericardium and the underlying heart move independently, where the underlying myocardium twists and the overlying pericardium does not (a relative "sliding" motion of the visceral and parietal pericardium). This can be visualized by using 1D- or 2D-tagged CMR. At end-diastole the tag lines cross both the pericardium and myocardium, and with systole, the visceral pericardial/myocardial tags move together and become displaced relative to the parietal pericardium and its tags in normal hearts. In cases of constriction, since the parietal pericardium is often adhered to the underlying visceral pericardium/myocardium, no sliding motion occurs, and the parietal pericardial tags remain aligned, and move and deform with, the visceral pericardium/myocardium and the associated tag lines. It is important to remember that constriction is a complex diagnosis and that the presence of pericardial adhesion(s) alone is not pathognomonic for the diagnosis.

Right Ventricular Function

The ability to accurately assess global and regional right ventricular (RV) function is very valuable in the study of diseases affecting the RV such as pulmonary hypertension, congenital heart disease, and arrhythmogenic RV dysplasia/cardiomyopathy (ARVD/C).

Fayad et al. [51] showed that in normal patients, RV regional shortening was not uniform, and in the pulmonary hypertension patients, both short- and long-axis regional shortening was decreased, most prominently in the RV outflow tract and the basal septum. In 21 patients with pulmonary arterial hypertension (PAH), high temporal resolution (14 ms) tagging MRI was performed, and Marcus et al. showed that there is left-to-right delay caused by lengthening of the duration of RV shortening, which is correlated with leftward septal bowing and decreased LV filling [92]. Voeller et al. further investigated RV strain change as a response to mild pressure overload versus severe pressure overload before the occurrence of RV dilation in a canine model [93]. They demonstrated that in mild RV pressure overload, there was no change in RV strain or function as compared to severe RV pressure overload, where there was a significant decrease in RV circumferential strain, with RV filling became dependent on the RV conduit function [93].

Bomma et al. [94] studied global and regional right and left ventricular function in patients with ARVD/C and found that global RV systolic function was reduced and RV volumes were increased in these patients as compared to controls. Both of these findings were more pronounced

toward the base of the RV. Tandri et al. [95] performed assessment of regional RV function in 20 patients with idiopathic right ventricular outflow tract (RVOT) tachycardia and found no difference in global and regional parameters as compared to controls. These results argue against the hypothesis that RVOT tachycardia may be an early form of ARVD/C.

In congenital heart disease, tagged CMR may provide a more quantitative approach to assessment of ventricular function that could permit more precise titration of medications or choice of surgical approaches based on long-term functional measures [96]. In a recent report of 372 patients with repaired tetralogy of Fallot, LV circumferential strain and RV longitudinal strain using feature tracking from cine images emerged as predictors of adverse outcome, independent of QRS duration, ejection fraction, ventricular volumes, New York Heart Association class, and peak oxygen uptake [97].

Conclusions

CMR methods are powerful tools for noninvasive assessment of regional left and right ventricular function. As modern cardiovascular care involves more difficult decision-making, the need exists for a greater understanding of the complex three-dimensional contractile patterns of both ventricles. An integrated knowledge of the effects of through-plane motion, torsional displacement, and strain measurements independent of incident ultrasound beam angle are only a few of the advances that modern CMR techniques have provided. The clinical applications for these methods continue to expand. Evaluation of cardiomyopathies, myocardial viability, ventricular remodeling, and assessment of patients for resynchronization therapy are examples of disorders where CMR has elucidated a new understanding of the mechanisms underlying these processes. More rapid acquisition and analysis methods, some of which are nearing clinical use, will further expand the clinical utility of these tools. The emergence of feature tracking techniques on cine CMR holds the potential to rapidly advance the application of myocardial regional assessment in heart diseases.

References

1. Holzapfel G. Nonlinear solid mechanics: a continuum approach for engineering. Chichester: Wiley; 2000.
2. Simpson RM, Keegan J, Firmin DN. MR assessment of regional myocardial mechanics. J Magn Reson Imaging. 2013;37(3):576–99.
3. Streeter DD Jr, Spotnitz HM, Patel DP, Ross J Jr, Sonnenblick EH. Fiber orientation in the canine left ventricle during diastole and systole. Circ Res. 1969;24(3):339–47.
4. LeGrice IJ, Smaill BH, Chai LZ, Edgar SG, Gavin JB, Hunter PJ. Laminar structure of the heart: ventricular myocyte arrangement and connective tissue architecture in the dog. Am J Phys. 1995;269(2 Pt 2):H571–82.
5. Schmid P, Jaermann T, Boesiger P, Niederer PF, Lunkenheimer PP, Cryer CW, et al. Ventricular myocardial architecture as visualised in postmortem swine hearts using magnetic resonance diffusion tensor imaging. Eur J Cardiothorac Surg. 2005;27(3):468–72.
6. Ingels NB Jr, Daughters GT 2nd, Stinson EB, Alderman EL, Miller DC. Three-dimensional left ventricular midwall dynamics in the transplanted human heart. Circulation. 1990;81(6):1837–48.
7. Arts T, Hunter WC, Douglas AS, Muijtjens AM, Corsel JW, Reneman RS. Macroscopic three-dimensional motion patterns of the left ventricle. Adv Exp Med Biol. 1993;346:383–92.
8. Ratcliffe MB, Gupta KB, Streicher JT, Savage EB, Bogen DK, Edmunds LH Jr. Use of sonomicrometry and multidimensional scaling to determine the three-dimensional coordinates of multiple cardiac locations: feasibility and initial implementation. IEEE Trans Biomed Eng. 1995;42(6):587–98.
9. Gorman JH 3rd, Gupta KB, Streicher JT, Gorman RC, Jackson BM, Ratcliffe MB, et al. Dynamic three-dimensional imaging of the mitral valve and left ventricle by rapid sonomicrometry array localization. J Thorac Cardiovasc Surg. 1996;112(3):712–26.
10. Wang H, Amini AA. Cardiac motion and deformation recovery from MRI: a review. IEEE Trans Med Imaging. 2012;31(2):487–503.
11. Ibrahim E-SH. Myocardial tagging by cardiovascular magnetic resonance: evolution of techniques – pulse sequences, analysis algorithms, and applications. J Cardiovasc Magn Reson. 2011;13:36.
12. Zerhouni EA, Parish DM, Rogers WJ, Yang A, Shapiro EP. Human heart: tagging with MR imaging – a method for noninvasive assessment of myocardial motion. Radiology. 1988;169(1):59–63.
13. Axel L, Dougherty L. MR imaging of motion with spatial modulation of magnetization. Radiology. 1989;171(3):841–5.
14. Xu C, Pilla JJ, Isaac G, Gorman JH 3rd, Blom AS, Gorman RC, et al. Deformation analysis of 3D tagged cardiac images using an optical flow method. J Cardiovasc Magn Reson. 2010;12:19.
15. Prince JL, McVeigh ER. Motion estimation from tagged MR image sequences. IEEE Trans Med Imaging. 1992;11(2):238–49.
16. Gupta SN, Prince J. On variable brightness optical flow for tagged MRI. Information Processing in Medical Imaging. 1995. p. 323–34.
17. Chandrashekara R, Mohiaddin RH, Rueckert D. Analysis of 3-D myocardial motion in tagged MR images using nonrigid image registration. IEEE Trans Med Imaging. 2004;23(10):1245–50.
18. Kerwin WS, Prince JL. Cardiac material markers from tagged MR images. Med Image Anal. 1998;2(4):339–53.
19. Amini AA, Chen Y, Elayyadi M, Radeva P. Tag surface reconstruction and tracking of myocardial beads from SPAMM-MRI with parametric B-spline surfaces. IEEE Trans Med Imaging. 2001;20(2):94–103.
20. Chen T, Wang X, Chung S, Metaxas D, Axel L. Automated 3D motion tracking using Gabor filter bank, robust point matching, and deformable models. IEEE Trans Med Imaging. 2010;29(1):1–11.
21. Osman NF, Kerwin WS, McVeigh ER, Prince JL. Cardiac motion tracking using CINE harmonic phase (HARP) magnetic resonance imaging. Magn Reson Med. 1999;42(6):1048–60.
22. Osman NF, McVeigh ER, Prince JL. Imaging heart motion using harmonic phase MRI. IEEE Trans Med Imaging. 2000;19(3):186–202.
23. Sampath S, Prince JL. Automatic 3D tracking of cardiac material markers using slice-following and harmonic-phase MRI. Magn Reson Imaging. 2007;25(2):197–208.
24. Arts T, Prinzen FW, Delhaas T, Milles JR, Rossi AC, Clarysse P. Mapping displacement and deformation of the heart with local sine-wave modeling. IEEE Trans Med Imaging. 2010;29(5):1114–23.
25. Lima JA, Jeremy R, Guier W, Bouton S, Zerhouni EA, McVeigh E, et al. Accurate systolic wall thickening by nuclear magnetic

resonance imaging with tissue tagging: correlation with sonomicrometers in normal and ischemic myocardium. J Am Coll Cardiol. 1993;21(7):1741–51.
26. Yeon SB, Reichek N, Tallant BA, Lima JA, Calhoun LP, Clark NR, et al. Validation of in vivo myocardial strain measurement by magnetic resonance tagging with sonomicrometry. J Am Coll Cardiol. 2001;38(2):555–61.
27. Young AA, Axel L, Dougherty L, Bogen DK, Parenteau CS. Validation of tagging with MR imaging to estimate material deformation. Radiology. 1993;188(1):101–8.
28. Moore CC, Reeder SB, McVeigh ER. Tagged MR imaging in a deforming phantom: photographic validation. Radiology. 1994;190(3):765–9.
29. Fischer SE, McKinnon GC, Maier SE, Boesiger P. Improved myocardial tagging contrast. Magn Reson Med. 1993;30(2):191–200.
30. Park J, Metaxas DN, Axel L, Yuan Q, Blom AS. Cascaded MRI-SPAMM for LV motion analysis during a whole cardiac cycle. Int J Med Inform. 1999;55(2):117–26.
31. Aletras AH, Ding S, Balaban RS, Wen H. DENSE: displacement encoding with stimulated echoes in cardiac functional MRI. J Magn Reson. 1999;137(1):247–52.
32. Feng L, Donnino R, Babb J, Axel L, Kim D. Numerical and in vivo validation of fast cine displacement-encoded with stimulated echoes (DENSE) MRI for quantification of regional cardiac function. Magn Reson Med. 2009;62(3):682–90.
33. Neizel M, Lossnitzer D, Korosoglou G, Schaufele T, Lewien A, Steen H, et al. Strain-encoded (SENC) magnetic resonance imaging to evaluate regional heterogeneity of myocardial strain in healthy volunteers: comparison with conventional tagging. J Magn Reson Imaging. 2009;29(1):99–105.
34. Bryant DJ, Payne JA, Firmin DN, Longmore DB. Measurement of flow with NMR imaging using a gradient pulse and phase difference technique. J Comput Assist Tomogr. 1984;8(4):588–93.
35. Pelc LR, Sayre J, Yun K, Castro LJ, Herfkens RJ, Miller DC, et al. Evaluation of myocardial motion tracking with cine-phase contrast magnetic resonance imaging. Investig Radiol. 1994;29(12):1038–42.
36. Paul J, Wundrak S, Bernhardt P, Rottbauer W, Neumann H, Rasche V. Self-gated tissue phase mapping using golden angle radial sparse SENSE. Magn Reson Med. 2016;75(2):789–800.
37. Schuster A, Kutty S, Padiyath A, Parish V, Gribben P, Danford DA, et al. Cardiovascular magnetic resonance myocardial feature tracking detects quantitative wall motion during dobutamine stress. J Cardiovasc Magn Reson. 2011;13:58.
38. Veress A, Weiss J, Rabbitt R, Lee J, Gullberg J. Measurement of 3D left ventricular strains during diastole using image warping and untagged MRI images. IEEE Comput Cardiol. 2001:165–8.
39. Sinusas AJ, Papademetris X, Constable RT, Dione DP, Slade MD, Shi P, et al. Quantification of 3-D regional myocardial deformation: shape-based analysis of magnetic resonance images. Am J Physiol Heart Circ Physiol. 2001;281(2):H698–714.
40. Hor KN, Gottliebson WM, Carson C, Wash E, Cnota J, Fleck R, et al. Comparison of magnetic resonance feature tracking for strain calculation with harmonic phase imaging analysis. JACC Cardiovasc Imaging. 2010;3(2):144–51.
41. Lu JC, Connelly JA, Zhao L, Agarwal PP, Dorfman AL. Strain measurement by cardiovascular magnetic resonance in pediatric cancer survivors: validation of feature tracking against harmonic phase imaging. Pediatr Radiol. 2014;44(9):1070–6.
42. Morton G, Schuster A, Jogiya R, Kutty S, Beerbaum P, Nagel E. Inter-study reproducibility of cardiovascular magnetic resonance myocardial feature tracking. J Cardiovasc Magn Reson. 2012;14:43.
43. Maret E, Todt T, Brudin L, Nylander E, Swahn E, Ohlsson JL, et al. Functional measurements based on feature tracking of cine magnetic resonance images identify left ventricular segments with myocardial scar. Cardiovasc Ultrasound. 2009;7:53.
44. Kuetting DL, Dabir D, Homsi R, Sprinkart AM, Luetkens J, Schild HH, et al. The effects of extracellular contrast agent (Gadobutrol) on the precision and reproducibility of cardiovascular magnetic resonance feature tracking. J Cardiovasc Magn Reson. 2016;18(1):30.
45. Schuster A, Stahnke VC, Unterberg-Buchwald C, Kowallick JT, Lamata P, Steinmetz M, et al. Cardiovascular magnetic resonance feature-tracking assessment of myocardial mechanics: Intervendor agreement and considerations regarding reproducibility. Clin Radiol. 2015;70(9):989–98.
46. Bistoquet A, Oshinski J, Skrinjar O. Left ventricular deformation recovery from cine MRI using an incompressible model. IEEE Trans Med Imaging. 2007;26(9):1136–53.
47. Clark NR, Reichek N, Bergey P, Hoffman EA, Brownson D, Palmon L, et al. Circumferential myocardial shortening in the normal human left ventricle. Assessment by magnetic resonance imaging using spatial modulation of magnetization. Circulation. 1991;84(1):67–74.
48. Fonseca CG, Oxenham HC, Cowan BR, Occleshaw CJ, Young AA. Aging alters patterns of regional nonuniformity in LV strain relaxation: a 3-D MR tissue tagging study. Am J Physiol Heart Circ Physiol. 2003;285(2):H621–30.
49. Oxenham HC, Young AA, Cowan BR, Gentles TL, Occleshaw CJ, Fonseca CG, et al. Age-related changes in myocardial relaxation using three-dimensional tagged magnetic resonance imaging. J Cardiovasc Magn Reson. 2003;5(3):421–30.
50. Hamdan A, Thouet T, Kelle S, Paetsch I, Gebker R, Wellnhofer E, et al. Regional right ventricular function and timing of contraction in healthy volunteers evaluated by strain-encoded MRI. J Magn Reson Imaging. 2008;28(6):1379–85.
51. Fayad ZA, Ferrari VA, Kraitchman DL, Young AA, Palevsky HI, Bloomgarden DC, et al. Right ventricular regional function using MR tagging: normals versus chronic pulmonary hypertension. Magn Reson Med. 1998;39(1):116–23.
52. Klein SS, Graham TP Jr, Lorenz CH. Noninvasive delineation of normal right ventricular contractile motion with magnetic resonance imaging myocardial tagging. Ann Biomed Eng. 1998;26(5):756–63.
53. Azhari H, Weiss JL, Rogers WJ, Siu CO, Shapiro EP. A noninvasive comparative study of myocardial strains in ischemic canine hearts using tagged MRI in 3-D. Am J Phys. 1995;268(5 Pt 2):H1918–26.
54. Denisova O, Shapiro EP, Weiss JL, Azhari H. Localization of ischemia in canine hearts using tagged rotated long axis MR images, endocardial surface stretch and wall thickening. Magn Reson Imaging. 1997;15(9):1037–43.
55. Kuijpers D, Ho KY, van Dijkman PR, Vliegenthart R, Oudkerk M. Dobutamine cardiovascular magnetic resonance for the detection of myocardial ischemia with the use of myocardial tagging. Circulation. 2003;107(12):1592–7.
56. Korosoglou G, Lossnitzer D, Schellberg D, Lewien A, Wochele A, Schaeufele T, et al. Strain-encoded cardiac MRI as an adjunct for dobutamine stress testing: incremental value to conventional wall motion analysis. Circ Cardiovasc Imaging. 2009;2(2):132–40.
57. Korosoglou G, Lehrke S, Wochele A, Hoerig B, Lossnitzer D, Steen H, et al. Strain-encoded CMR for the detection of inducible ischemia during intermediate stress. JACC Cardiovasc Imaging. 2010;3(4):361–71.
58. Kido T, Nagao M, Kurata A, Miyagawa M, Ogimoto A, Mochizuki T. Stress/rest circumferential strain in non-ischemia, ischemia, and infarction – quantification by 3 Tesla tagged magnetic resonance imaging. Circ J. 2013;77(5):1235–41.
59. Bogaert J, Bosmans H, Maes A, Suetens P, Marchal G, Rademakers FE. Remote myocardial dysfunction after acute anterior myocardial infarction: impact of left ventricular shape on regional function: a

magnetic resonance myocardial tagging study. J Am Coll Cardiol. 2000;35(6):1525–34.
60. Marcus JT, Gotte MJ, Van Rossum AC, Kuijer JP, Heethaar RM, Axel L, et al. Myocardial function in infarcted and remote regions early after infarction in man: assessment by magnetic resonance tagging and strain analysis. Magn Reson Med. 1997;38(5):803–10.
61. Gotte MJ, van Rossum AC, Marcus JT, Kuijer JP, Axel L, Visser CA. Recognition of infarct localization by specific changes in intramural myocardial mechanics. Am Heart J. 1999;138(6 Pt 1):1038–45.
62. Gerber BL, Rochitte CE, Melin JA, McVeigh ER, Bluemke DA, Wu KC, et al. Microvascular obstruction and left ventricular remodeling early after acute myocardial infarction. Circulation. 2000;101(23):2734–41.
63. Neizel M, Lossnitzer D, Korosoglou G, Schaufele T, Peykarjou H, Steen H, et al. Strain-encoded MRI for evaluation of left ventricular function and transmurality in acute myocardial infarction. Circ Cardiovasc Imaging. 2009;2(2):116–22.
64. Baer FM, Voth E, Schneider CA, Theissen P, Schicha H, Sechtem U. Comparison of low-dose dobutamine-gradient-echo magnetic resonance imaging and positron emission tomography with [18F] fluorodeoxyglucose in patients with chronic coronary artery disease. A functional and morphological approach to the detection of residual myocardial viability. Circulation. 1995;91(4):1006–15.
65. Sayad DE, Willett DL, Hundley WG, Grayburn PA, Peshock RM. Dobutamine magnetic resonance imaging with myocardial tagging quantitatively predicts improvement in regional function after revascularization. Am J Cardiol. 1998;82(9):1149–51. A10
66. Bree D, Wollmuth JR, Cupps BP, Krock MD, Howells A, Rogers J, et al. Low-dose dobutamine tissue-tagged magnetic resonance imaging with 3-dimensional strain analysis allows assessment of myocardial viability in patients with ischemic cardiomyopathy. Circulation. 2006;114(1 Suppl):I33–6.
67. Geskin G, Kramer CM, Rogers WJ, Theobald TM, Pakstis D, Hu YL, et al. Quantitative assessment of myocardial viability after infarction by dobutamine magnetic resonance tagging. Circulation. 1998;98(3):217–23.
68. Choudhury L, Mahrholdt H, Wagner A, Choi KM, Elliott MD, Klocke FJ, et al. Myocardial scarring in asymptomatic or mildly symptomatic patients with hypertrophic cardiomyopathy. J Am Coll Cardiol. 2002;40(12):2156–64.
69. Young AA, Kramer CM, Ferrari VA, Axel L, Reichek N. Three-dimensional left ventricular deformation in hypertrophic cardiomyopathy. Circulation. 1994;90(2):854–67.
70. Kramer CM, Reichek N, Ferrari VA, Theobald T, Dawson J, Axel L. Regional heterogeneity of function in hypertrophic cardiomyopathy. Circulation. 1994;90(1):186–94.
71. Kim YJ, Choi BW, Hur J, Lee HJ, Seo JS, Kim TH, et al. Delayed enhancement in hypertrophic cardiomyopathy: comparison with myocardial tagging MRI. J Magn Reson Imaging. 2008;27(5):1054–60.
72. Bogarapu S, Puchalski MD, Everitt MD, Williams RV, Weng HY, Menon SC. Novel cardiac magnetic resonance feature tracking (CMR-FT) analysis for detection of myocardial fibrosis in pediatric hypertrophic cardiomyopathy. Pediatr Cardiol. 2016;37(4):663–73.
73. Ennis DB, Epstein FH, Kellman P, Fananapazir L, McVeigh ER, Arai AE. Assessment of regional systolic and diastolic dysfunction in familial hypertrophic cardiomyopathy using MR tagging. Magn Reson Med. 2003;50(3):638–42.
74. Palmon LC, Reichek N, Yeon SB, Clark NR, Brownson D, Hoffman E, et al. Intramural myocardial shortening in hypertensive left ventricular hypertrophy with normal pump function. Circulation. 1994;89(1):122–31.
75. Rosen BD, Edvardsen T, Lai S, Castillo E, Pan L, Jerosch-Herold M, et al. Left ventricular concentric remodeling is associated with decreased global and regional systolic function: the Multi-Ethnic Study of Atherosclerosis [see comment]. Circulation. 2005;112(7):984–91.
76. Edvardsen T, Rosen BD, Pan L, Jerosch-Herold M, Lai S, Hundley WG, et al. Regional diastolic dysfunction in individuals with left ventricular hypertrophy measured by tagged magnetic resonance imaging – the Multi-Ethnic Study of Atherosclerosis (MESA). Am Heart J. 2006;151(1):109–14.
77. MacGowan GA, Shapiro EP, Azhari H, Siu CO, Hees PS, Hutchins GM, et al. Noninvasive measurement of shortening in the fiber and cross-fiber directions in the normal human left ventricle and in idiopathic dilated cardiomyopathy. Circulation. 1997;96(2):535–41.
78. Nelson GS, Curry CW, Wyman BT, Kramer A, Declerck J, Talbot M, et al. Predictors of systolic augmentation from left ventricular preexcitation in patients with dilated cardiomyopathy and intraventricular conduction delay. Circulation. 2000;101(23):2703–9.
79. Young AA, Dokos S, Powell KA, Sturm B, McCulloch AD, Starling RC, et al. Regional heterogeneity of function in nonischemic dilated cardiomyopathy. Cardiovasc Res. 2001;49(2):308–18.
80. Joseph S, Moazami N, Cupps BP, Howells A, Craddock H, Ewald G, et al. Magnetic resonance imaging-based multiparametric systolic strain analysis and regional contractile heterogeneity in patients with dilated cardiomyopathy. J Heart Lung Transplant. 2009;28(4):388–94.
81. Han Y, Chan J, Haber I, Peters DC, Zimetbaum PJ, Manning WJ, et al. Circumferential myocardial strain in cardiomyopathy with and without left bundle branch block. J Cardiovasc Magn Reson. 2010;12:2.
82. Kanzaki H, Nakatani S, Yamada N, Urayama S, Miyatake K, Kitakaze M. Impaired systolic torsion in dilated cardiomyopathy: reversal of apical rotation at mid-systole characterized with magnetic resonance tagging method. Basic Res Cardiol. 2006;101(6):465–70.
83. Stuber M, Scheidegger MB, Fischer SE, Nagel E, Steinemann F, Hess OM, et al. Alterations in the local myocardial motion pattern in patients suffering from pressure overload due to aortic stenosis. Circulation. 1999;100(4):361–8.
84. Nagel E, Stuber M, Burkhard B, Fischer SE, Scheidegger MB, Boesiger P, et al. Cardiac rotation and relaxation in patients with aortic valve stenosis [see comment]. Eur Heart J. 2000;21(7):582–9.
85. Sandstede JJW, Johnson T, Harre K, Beer M, Hofmann S, Pabst T, et al. Cardiac systolic rotation and contraction before and after valve replacement for aortic stenosis: a myocardial tagging study using MR imaging. AJR Am J Roentgenol. 2002;178(4):953–8.
86. Ungacta FF, Davila-Roman VG, Moulton MJ, Cupps BP, Moustakidis P, Fishman DS, et al. MRI-radiofrequency tissue tagging in patients with aortic insufficiency before and after operation. Ann Thorac Surg. 1998;65(4):943–50.
87. Pomerantz BJ, Wollmuth JR, Krock MD, Cupps BP, Moustakidis P, Kouchoukos NT, et al. Myocardial systolic strain is decreased after aortic valve replacement in patients with aortic insufficiency. Ann Thorac Surg. 2005;80(6):2186–92.
88. Mankad R, McCreery CJ, Rogers WJ Jr, Weichmann RJ, Savage EB, Reichek N, et al. Regional myocardial strain before and after mitral valve repair for severe mitral regurgitation. J Cardiovasc Magn Reson. 2001;3(3):257–66.
89. Maniar HS, Brady BD, Lee U, Cupps BP, Kar J, Wallace KM, et al. Early left ventricular regional contractile impairment in chronic mitral regurgitation occurs in a consistent, heterogeneous pattern. J Thorac Cardiovasc Surg. 2014;148(4):1694–9.
90. Bogaert J, Maes A, Van De WF, Bosmans H, Herregods MC, Nuyts J, et al. Functional recovery of subepicardial myocardial tissue in transmural myocardial infarction after successful reperfusion: an important contribution to the improvement of regional and global left ventricular function. Circulation. 1999;99(1):36–43.
91. Kojima S, Yamada N, Goto Y. Diagnosis of constrictive pericarditis by tagged cine magnetic resonance imaging. N Engl J Med. 1999;341(5):373–4.

92. Marcus JT, Gan CT, Zwanenburg JJ, Boonstra A, Allaart CP, Gotte MJ, et al. Interventricular mechanical asynchrony in pulmonary arterial hypertension: left-to-right delay in peak shortening is related to right ventricular overload and left ventricular underfilling. J Am Coll Cardiol. 2008;51(7):750–7.
93. Voeller RK, Aziz A, Maniar HS, Ufere NN, Taggar AK, Bernabe NJ Jr, et al. Differential modulation of right ventricular strain and right atrial mechanics in mild vs. severe pressure overload. Am J Physiol Heart Circ Physiol. 2011;301(6):H2362–71.
94. Bomma C, Dalal D, Tandri H, Prakasa K, Nasir K, Roguin A, et al. Regional differences in systolic and diastolic function in arrhythmogenic right ventricular dysplasia/cardiomyopathy using magnetic resonance imaging. Am J Cardiol. 2005;95(12):1507–11.
95. Tandri H, Bluemke DA, Ferrari VA, Bomma C, Nasir K, Rutberg J, et al. Findings on magnetic resonance imaging of idiopathic right ventricular outflow tachycardia. Am J Cardiol. 2004;94(11):1441–5.
96. Menteer J, Weinberg PM, Fogel MA. Quantifying regional right ventricular function in tetralogy of Fallot. J Cardiovasc Magn Reson. 2005;7(5):753–61.
97. Orwat S, Diller GP, Kempny A, Radke R, Peters B, Kuhne T, et al. Myocardial deformation parameters predict outcome in patients with repaired tetralogy of Fallot. Heart. 2016;102(3):209–15.